Piezospectroscopy and first-principles calculations of the nitrogen-vacancy center in gallium arsenide

Nicola Kovac, Christopher Künneth, and Hans Christian Alt[a)]
Department of Applied Sciences and Mechatronics, Munich University of Applied Sciences, Lothstr. 34, D-80335 Munich, Germany

(Received 31 October 2017; accepted 12 January 2018; published online 31 January 2018)

The nitrogen-vacancy (NV) center occurs in GaAs bulk crystals doped or implanted with nitrogen. The local vibration of nitrogen gives rise to a sharp infrared absorption band at 638 cm^{-1}, exhibiting a fine structure due to the different masses of neighboring ^{69}Ga and ^{71}Ga host isotopes. Piezospectroscopic investigations in the crystallographic ⟨100⟩ direction prove that the center has C_{3v} point symmetry, which is weakly perturbed by the isotope effect. The stress-induced shifts of some band components show an unusual non-linear behavior that can be explained by coupling between the isotope and the stress splitting. First-principles density-functional theory calculations are in full accordance with the experiments and confirm the C_{3v} symmetry, caused by relaxation of the nitrogen atom from the anion lattice site towards the nearest-neighbor Ga plane. Furthermore, the calculations indicate the –3 charge state of the center as the most stable one for nearly all Fermi level positions. The NV center in GaAs is structurally analogous to the same center in diamond. *Published by AIP Publishing.* https://doi.org/10.1063/1.5011302

I. INTRODUCTION

Nitrogen is of continuing interest as a dopant in GaAs. Renewed research activities have been initiated due to the development of dilute nitrides, in particular, of the alloys $GaAs_{1-x}N_x$ and $Ga_{1-y}In_yAs_{1-x}N_x$, with N fractions up to a few percent.[1] The incorporation of nitrogen on the anion lattice site (N_{As}) leads to a strong narrowing of the bandgap of initially 180 meV per percent of nitrogen. There is a great technological interest in these alloys, driven by the search for optimized materials for lasers emitting at 1.3 and 1.55 μm as well as multi-junction solar cells.[2,3]

The importance of nitrogen as a luminescent center in GaAs has been first put forward in 1985, when luminescence from isoelectronic N and NN pairs was detected in N doped GaAs layers under pressure,[4] and later by more extensive macro- and micro-photoluminescence studies.[5,6] Recently, a nitrogen-related center acting as a single-photon emitter has been reported from nitrogen delta-doped layers in GaAs. These centers might be of interest for future quantum information processing.[7,8]

These material issues of N in the GaAs lattice are primarily concerned with isoelectronic substitutional nitrogen. Consequently, detailed theoretical investigations of the formation of isolated N, different NN pairs, and N clusters have been carried out.[9] However, interstitial N and complexes of N with Ga and As atoms and with intrinsic defects (interstitials, vacancies) also play an important role in these applications, as evidenced both theoretically and experimentally.[10–12]

Nitrogen-related defects in GaAs can be investigated by local vibrational mode (LVM) spectroscopy due to the small mass of the N atom compared to the Ga and As atoms of the lattice. The isolated substitutional nitrogen atom on anion site, N_{As}, gives rise to a relatively broad unstructured LVM band at 471.5 cm^{-1} (low temperatures).[13,14]

Another LVM band at 638 cm^{-1}, first tentatively associated with nitrogen impurities due to its appearance in nitrogen-rich crystals,[15] is caused by the $N_{As} - V_{Ga}$ nearest-neighbor pair, the nitrogen-vacancy (NV) center in GaAs.[16] It occurs in both GaAs bulk material doped with a high concentration of N and in N-implanted GaAs layers. The LVM at 638 cm^{-1} splits at low temperature into four components due to the mass effect of the different host isotopes ^{69}Ga and ^{71}Ga, acting as nearest neighbors of the substitutional nitrogen atom. An empirical valence-force model (VFM) was given which reproduces the fine structure of the 638 cm^{-1}-LVM both qualitatively and quantitatively.[16] The analysis is based on a twofold degenerate E (transverse) mode of a trigonal center with C_{3v} symmetry, weakly perturbed by the different Ga host isotope masses. Finally, it should be mentioned that the related nitrogen-hydrogen-vacancy center, incorporating additionally one hydrogen atom, was also investigated by LVM spectroscopy.[17]

In this work, an extensive study on the atomistic structure, energetics, and vibrational properties of the NV center in GaAs is presented. We performed Fourier transform infrared (FTIR) absorption measurements on the 638 cm^{-1}-band under uniaxial stress in the ⟨100⟩ direction to get further experimental information on the defect symmetry. Second, density-functional theory (DFT) calculations of the minimum energy configurations in different charge states were carried out to calculate the formation energy and the associated LVM frequencies.

II. EXPERIMENTAL AND COMPUTATIONAL METHODS

Samples investigated were prepared from a nitrogen-doped GaAs crystal grown by the liquid-encapsulation

[a)]Electronic mail: hchalt@hm.edu

Czochralski technique. Nitrogen doping was achieved by applying a N_2 gas atmosphere of 70 bar during crystal growth. For uniaxial stress experiments, rod-like specimens with a typical size of 2 mm × 4 mm × 10 mm were cut with alignment of the long axis parallel to the crystallographic [0 0 1] direction. Uniaxial stress measurements up to 0.15 GPa were performed using home-made push-rod apparatus inside an optical helium cryostat. The force on the mounted sample was provided by a pressure intensifier coupled to the apparatus. The absolute value of stress was set by the nitrogen gas pressure on the low-pressure side of the pressure intensifier, which was monitored by a precision gauge. Fourier transform infrared (FTIR) measurements were performed with a vacuum instrument (Bruker Vertex 80v), equipped with a potassium bromide (KBr) beam splitter and a liquid-nitrogen cooled mercury cadmium telluride (MCT) detector. The absorption spectra were taken with an apodized spectral resolution of 0.08 cm^{-1}. A wire-grid polarizer in front of the cryostat was used to obtain polarized spectra.

The minimum-energy structures were obtained with the all-electron DFT code FHI-Aims[18–22] which utilizes numeric atom-centered basis functions. The tight basis set on the "Second tier"-level in the local density approximation (LDA) approximation (PW[23] parameterization) was used for all calculations in this publication. A pure GaAs super cell with 64 atoms Ga_{32} As_{32} and $F\bar{4}3m$ (No. 216) symmetry was set up as the host crystal for the N_{As} V_{Ga} (NV) center (63 atoms for NV, Ga_{31} As_{31} N). A k-point grid of 3 × 3 × 3 was used, and the atomic positions and lattice constants were relaxed until the forces fell below 5×10^{-5} eV/Å and 5×10^{-4} eV/Å for the electronic and ionic forces, respectively. Only in the case of charged ($q \neq 0$) super cells, the lattice constants were kept fixed at the uncharged values, relaxing only the atomic positions.

Formation energies were calculated according to[24]

$$\begin{aligned} E^{\mathrm{f}}[\mathrm{NV}^q] = {} & E_{\mathrm{tot}}[\mathrm{NV}^q] - E_{\mathrm{tot}}[\mathrm{GaAs}] \\ & + \mu_{\mathrm{N}} - \mu_{\mathrm{As}} - \mu_{\mathrm{Ga}} \\ & + q\left(E_{\mathrm{F}} + E_{\mathrm{VBM}}[\mathrm{GaAs}] + \Delta V[\mathrm{NV}^0]\right) \\ & + E_{\mathrm{corr}}[\mathrm{NV}^q], \end{aligned} \tag{1}$$

with E^{f} the formation energy, E_{tot} the total energies, μ the chemical potentials, E_{F} the Fermi level referenced to the energy of the valence band maximum E_{VBM}, ΔV the potential alignment, and E_{corr} the charge correction due to finite size of the unit cell. E_{corr} was calculated with the scaling law[25] $E_{\mathrm{f}} \sim a/L + c$ using 216 atomic supercells. a and c are fit parameters and L is the size of the super cell. Charged structures were considered for the charges $q/e = -4, \ldots, +4$, with the lattice constants fixed to the uncharged structure. μ_{As} was calculated from trigonal metallic As, μ_{Ga} from metallic α-Ga, and μ_{N} from the N_2 molecule.

Figures of the atomic structures in this publication are produced with Ovito.[26] Vibrational frequencies were obtained with the utility Phonopy[27] using finite displacements. Isotope-dependent vibrational frequencies were calculated by changing the masses in the denominator of the dynamical matrix before solving the eigenvalue problem. The calculated vibrational frequencies (ω_{calc}) were scaled to the experimental frequencies (ω_{exp}) with the scaling factor $c = (\sum_i \omega_{i,\mathrm{calc}} \omega_{i,\mathrm{exp}}) / \sum_i \omega_{i,\mathrm{calc}}^2$ according to Ref. 28.

III. RESULTS AND DISCUSSION

A. Piezospectroscopic experiments

Series of polarized absorption spectra of the 638 cm^{-1}-band for different stresses σ parallel to the [1 0 0] direction are displayed in Fig. 1. At zero stress, the band has the known quadruplet fine structure originating from the isotopic perturbation of the LVM frequency by the different gallium host isotopes (^{69}Ga and ^{71}Ga) as nearest neighbours of the nitrogen atom (^{14}N). The corresponding isotopic configurations and LVM frequencies are listed in Table I. The peak-to-peak separation of the four lines is about 0.24 cm^{-1}, and the full width at half-maximum (FWHM) amounts to 0.11(1) cm^{-1}.

With increasing stress, all components of the band shift to higher frequencies. The individual line shifts are very small and lie between 0.1 and 0.5 cm^{-1} per 0.1 GPa. Moreover, some components show a splitting and others an apparent broadening with increasing stress. The line splitting is especially clearly seen in the series of perpendicularly polarized spectra at intermediate stresses, whereas for parallel polarization this behavior is sometimes obscured by apparent broadening. However, the apparent line broadening as well as the simultaneous increase or decrease of line intensities can in fact be attributed completely to stress-induced splitting. As some lines still have a well-defined resolved line shape (e.g., at 0.15 GPa for the (E⊥ σ) case), line broadening due to inhomogeneous stress fields inside the specimen occurs only to a minimal extent. From careful spectra analysis, we estimate this increased width (FWHM) to about 18% at highest stresses. Therefore, we assume that in both polarization directions the observed apparent line broadening results from overlapping of stress-split lines. Furthermore, comparison of the matching ($E \perp \sigma$) and ($E \parallel \sigma$) spectra shows that some split

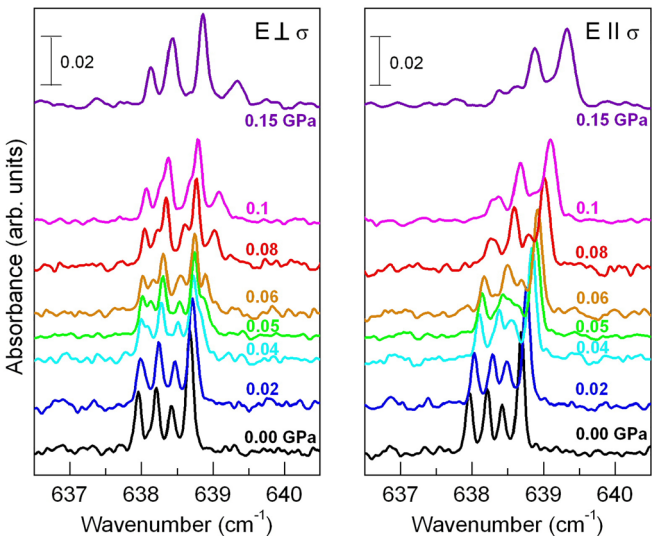

FIG. 1. Effect of ⟨100⟩ stress on the fine structure of the 638 cm^{-1}-band for both polarization directions. Sample temperature is 10 K and the spectral resolution is 0.08 cm^{-1}.

TABLE I. NV center/638 cm^{-1}-band: Isotopic combinations and point symmetries, LVM symmetry types, weighted probabilities, frequencies, stress-induced splitting, and polarization behavior. The calculated vibrational frequencies are for charge $q/e = -3$ and scaled with a factor of $c = 0.9862$.

Configuration (notation)	Point symmetry	LVM symm. type (degeneracy)	Weighted probability[a]	Frequency/cm^{-1} calc. (meas.)	Frequency shift ⟨100⟩ stress[b]	Intensity ratio $I_\parallel : I_\perp$	Intensity ratio $I_\parallel : I_\perp$[c]
$^{14}N^{71}Ga_3$	C_{3v}	E (2)	0.0635	637.93 (637.95)	$(A_\alpha - 2B_\alpha)\sigma$	4:1	
(α)					$(A_\alpha + 2B_\alpha)\sigma$	0:3	
$^{14}N^{71}Ga_2{}^{69}Ga_1$	C_s	A' (1)	0.1435	638.43 (638.41)	$A_{\beta 1}\sigma$	8/3:2/3	
(β)					$A_{\beta 2}\sigma$	4/3:10/3	16/3:4/3
		A'' (1)	0.1435	637.94 (637.95)	$A_{\beta 3}\sigma$	0:2	
					$A_{\beta 4}\sigma$	4:2	0:4
$^{14}N^{71}Ga_1{}^{69}Ga_2$	C_s	A' (1)	0.2162	638.19 (638.20)	$A_{\gamma 1}\sigma$	8/3:2/3	
(γ)					$A_{\gamma 2}\sigma$	4/3:10/3	16/3:4/3
		A'' (1)	0.2162	638.67 (638.67)	$A_{\gamma 3}\sigma$	0:2	
					$A_{\gamma 4}\sigma$	4:2	0:4
$^{14}N^{69}Ga_3$	C_{3v}	E (2)	0.2172	638.69 (638.67)	$(A_\delta - 2B_\delta)\sigma$	4:1	
(δ)					$(A_\delta + 2B_\delta)\sigma$	0:3	

[a]Calculated with the natural abundances of ^{69}Ga and ^{71}Ga of 0.61 and 0.39, respectively.
[b]Parameters A and B given in Table II.
[c]Limiting case of complete stress-induced eigenvector rotation.

components are only partially polarized. Therefore, a clear visual separation and identification of the individual lines is not possible. That is why we started to evaluate the stress-induced splittings by curve-fitting methods, following the theoretical predictions of the piezospectroscopic behavior.

The NV center has four different isotopic configurations due to the different combinations of the nearest-neighbor Ga atoms (Table I) as well as four different orientations within the unit cell of the zinc-blende structure (Fig. 2).[16] Both isotopically pure configurations have C_{3v} symmetry and a two-fold degenerate E mode, whereas both mixed configurations have C_s symmetry and two non-degenerate modes of type A' and A''. The characteristics of the uniaxial stress effect on non-degenerate states in cubic crystals have been given by Kaplyanskii.[29] The corresponding theory for doubly degenerate states in tetragonal and trigonal centers has been developed and applied to specific cases in Refs. 30–32.

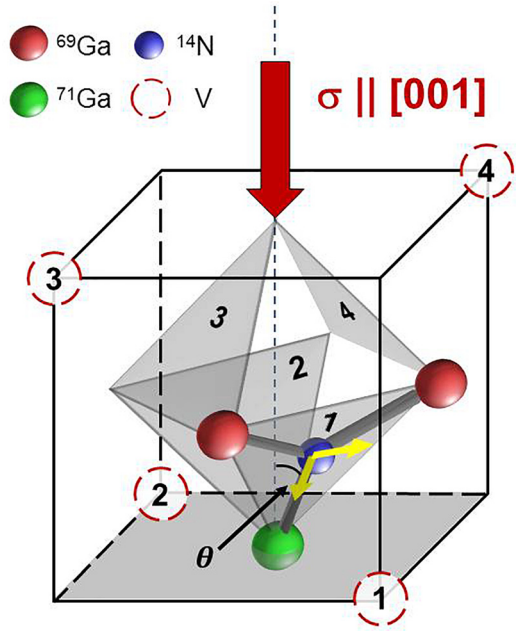

FIG. 2. Schematic picture of the geometry and orientations of the NV complex (assumed to be planar, see text for discussion) in the GaAs lattice. The possible vacancy positions are labelled by 1, 2, 3, and 4. The Ga plane forms an angle θ with the [001] stress direction. In isotopically mixed configurations (as shown here), the different possible orientations of the eigenvector (yellow arrows) for the A' and A'' mode have to be taken into account for IR intensity calculations.

For ⟨100⟩ stress, each of the A' and A'' modes splits into two branches, due to partial lifting of orientational degeneracy.[29] The relative intensities for polarization parallel and perpendicular to the stress direction depend on the orientation of the dipole vector, given by the angle θ' between this vector and the ⟨100⟩ stress direction. The general case has been treated in Ref. 32. The Ga plane of the NV center forms an angle $\theta = \cos^{-1}(\sqrt{2/3}) = 35.26°$ with the applied stress direction (see Fig. 2). From this angle θ and the specific isotope configuration, all possible angles θ' are easily calculated. The resulting intensity ratios under polarized light are given in Table I. For the E mode, the theory requires a splitting into two branches, corresponding to its two eigenstates, and thus to a total lifting of its intrinsic degeneracy. The orientational degeneracy is not lifted as all orientations are equivalent with respect to the ⟨100⟩ axis (Fig. 2). Intensity ratios are also listed in Table I.

In accordance with these considerations, the required number of stress-split lines was fitted to the spectra shown in Fig. 1. The appropriate line intensities under polarized light were calculated from the spectrum at zero pressure, taking into account the relative intensity ratios given in Table I. Line shapes were described by a mixed Gaussian-Lorentzian function with an initial FWHM of 0.11 cm^{-1}. The small stress-induced line broadening (see above) was approximated by a linear increase of the FWHM of 0.133 cm^{-1}/GPa and a proportional decrease of intensity.

B. Linear and non-linear stress dependencies

For low stresses, the fitted curves resulting from the linear stress dependencies listed in Table I are in good

agreement with the measured spectra. However, from 0.05 GPa upwards, increasingly significant divergences between fitted and measured lines are obvious in some parts of the spectra [Figs. 3(a) and 3(b)]. In both polarization directions, however, in particular, for parallel polarization, lacking or excessive intensity appears within the adjusted curves. As the integrated absorbance has to be constant for all applied stresses, we must assume a stress-induced change of the intensities. Moreover, a systematic change of the stress-induced line shifts at higher stresses can be visualized from a plot of the curve fitting results so far (see Fig. 7). It shows that shifts of all lines depend linearly on the stress up to roughly 0.05 GPa. However, starting from this stress value, four lines belonging to one branch of each A' and A'' mode deviate from their initially linear behavior, indicating a non-linear contribution to the shift.

Thus, a partial failure of the linear line-shift model is evident. Based on the observations mentioned above, these problems must be assigned to the A' and A'' modes, originating from the mixed-isotope configurations β and γ. The physical reason behind this is the fact that these modes are basically E modes which are split by two weak symmetry-lowering perturbations: (i) the deviation from C_{3v} symmetry due to the two different Ga isotopes and (ii) the deviation from C_{3v} symmetry due to the stress in $\langle 100 \rangle$ direction. In the present case, both effects are of the same order of magnitude. The former leads to an orientation of the two orthogonal eigenvectors ($\vec{e}_H$ and $\vec{e}_L$) of the E mode parallel and perpendicular to the corresponding Ga isotopes (see Fig. 2 for one particular case). The latter tries to re-orient the two orthogonal eigenvectors such that one (with the lower frequency) is perpendicular to the stress direction.

To get more insight into the competing influences of these two perturbations, it was considered necessary to use a simulation with the empirical valence-force model (VFM) of the NV complex given earlier.[16] In this model, the defect is approximated by a planar NGa_3 molecule, orientated as shown in Fig. 2. For simulating the applied stress, the force constant of the N-Ga bond including the smallest angle (θ) with the $\langle 001 \rangle$ direction was increased whereas the other two force constants were kept unchanged (see Fig. 5). All three possibilities to distribute two ^{71}Ga and one ^{69}Ga (β) or one ^{71}Ga and two ^{69}Ga (γ), respectively, on the three Ga lattice sites were considered. By solving the dynamical matrix, the shift of the eigenfrequencies and the re-orientation of the eigenvectors of the vibrating system could be traced systematically as a function of stress.

The results for the eigenfrequencies are shown in Fig. 4. In agreement with general theory,[29] the simulation predicts the splitting of each A' and A'' mode into two branches. In all four cases, this pair consists of one branch with linear and one with non-linear stress dependence. The linear branches derive from the case where the eigenvector of the low-frequency mode is at zero stress perpendicular to the $\langle 100 \rangle$ direction [see Fig. 5(a)], whereas the non-linear whereas the non-linear branches represent the cases where this is not true [see Fig. 5(b)]. In these latter cases, the non-linear behavior is due to the fact that the mode eigenvector starts rotating immediately after applying $\langle 100 \rangle$ stress. As this rotation is a non-linear function of the applied stress, also the frequency shift is non-linear. For both isotopically mixed configurations, the eigenvector rotation continues with increasing stress until finally the low-frequency mode is orientated perpendicular to the $\langle 100 \rangle$ stress axis (Fig. 5). Therefore, the stress-induced shift of the non-linear branches approximates asymptotically one of the linear branches, as observable in Fig. 4, leading finally to equal slopes.

Correlated with the mode eigenvector rotation is a change of the absorption intensity under polarized light because of the corresponding rotation of the electric dipole vector. To get an estimate of the size of this effect, we compared the simulated and measured line shifts. Thereby we could approximately assign the experimentally applied stresses values to the relative force constant changes in the VFM simulations (see Fig. 4).The relative changes of the

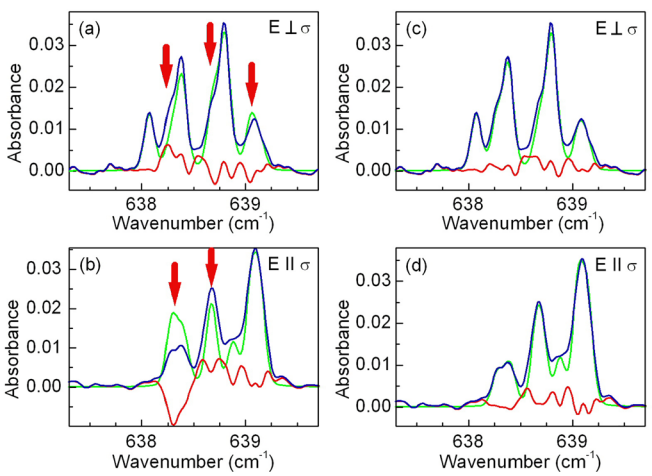

FIG. 3. Fitting results of the 638 cm^{-1}-band at 0.1 GPa (blue line: measured spectrum, green line: fitted curve, and red line: difference). Linear [(a) and (b)] and the improved [(c) and (d)] line-shift model of the A' and A'' modes. Significant discrepancies between the linear fit and the measured spectra are highlighted by arrows.

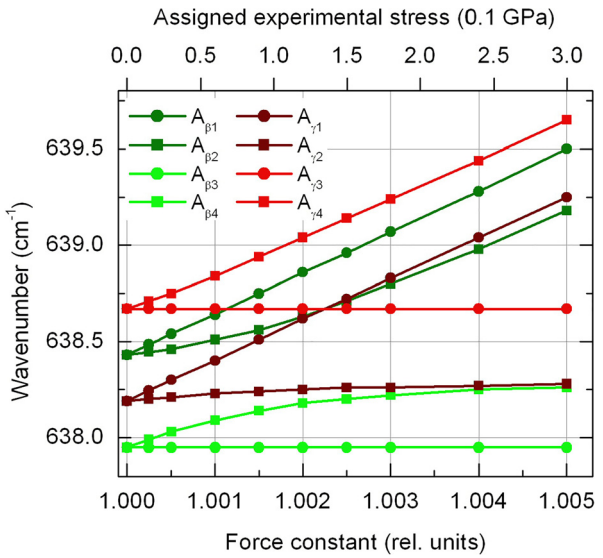

FIG. 4. Stress-induced frequency shifts of the A' and A'' modes simulated by the valence-force model of the NV complex (circle: linear branch; square: non-linear branch).

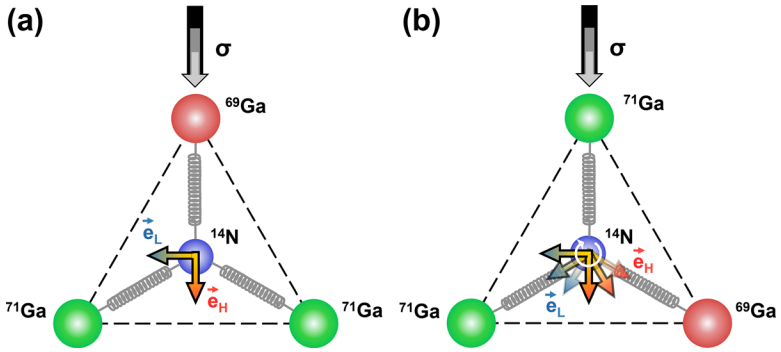

FIG. 5. Schematic picture of the stress-induced eigenvector rotation for the isotopically mixed NGa_3 configurations. The occurrence of this effect depends on the initial orientation of the high- and low-frequency eigenvectors $\vec{e}_H$ and $\vec{e}_L$ relative to the stress direction [compare (a) and (b)].

modified line intensities according to this approach are shown for both polarization directions in Fig. 6. Theses corrected intensities of the four non-linear A' and A'' modes were used to fit the spectra for stresses larger than 0.04 GPa. Fitted spectra are now in satisfying agreement with the measured spectra [Figs. 3(c) and 3(d)]. Residual deviations are mostly not larger than background fluctuations.

The complete results of the fitting procedure are illustrated in Fig. 7. The fitted frequency shifts are visualized by second-order polynomials. Splitting of the six modes of the NV complex into two branches each is clearly observable. The splitting originates either from total lifting of the intrinsic degeneracy in the case of the twofold degenerate E modes, being typical for $A \rightarrow E$ transitions in centers of C_{3v} symmetry for $\langle 100 \rangle$ stress, or from partial lifting of the orientational degeneracy in the case of the A' and A'' modes, being typical for $A \rightarrow A$ transitions in centers of C_s symmetry under the same conditions.

All branches exhibit a linear stress-induced frequency shift, apart from the four branches belonging to the A' and A'' modes with eigenvector rotation, as discussed above. In these cases, the initial (linear) slopes ($\sigma < 0.05$ GPa) were fitted separately (see dashed lines in Fig. 7). The slopes of two E mode branches are pairwise practically identical within the accuracy given by experiment. Indeed, it turns out that the numerical values for all slopes, when regarding the asymptotic behavior of the non-linear branches, fall into two groups: one with a slope of about 1.2 cm^{-1}/GPa and another

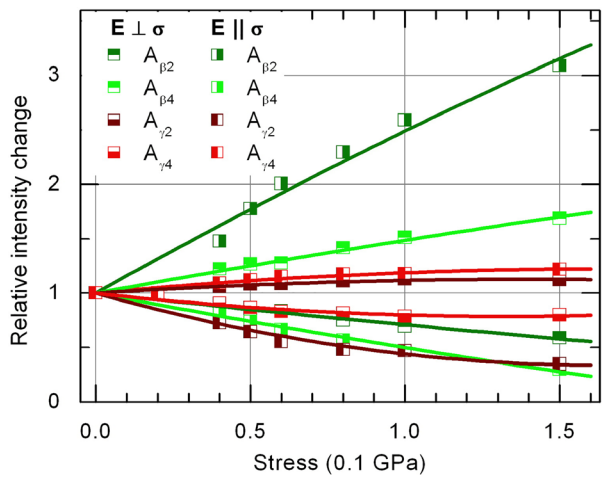

FIG. 6. Relative intensity change due to rotation of the eigenvector of the non-linear A′ and A″ branches as a function of applied stress.

with about 4.6 cm^{-1}/GPa. This circumstance is not unexpected due to the fact that the different vibrational modes of the NV complex originate from defects being identical in structure and bonding chemistry, perturbed only slightly by the different Ga isotope combinations. Finally, all these results (splitting, shift and polarization behavior) confirm the point symmetry of the different isotope configurations for the NV complex in GaAs, given in Table I. The corresponding piezospectroscopic parameters, derived from the linear parts of the fitted polynomials, are listed in Table II.

C. First-principles calculations

The starting structure for the DFT calculations was a 63-atom super cell prepared from a zinc-blende structure with 64 atoms by substituting an N atom for an As atom and removing one of the adjacent Ga atoms. The structure was converged without using symmetry constraints. The final positions in the environment of the nitrogen atom are illustrated in Fig. 8. During optimization, the N atom moves towards the center of the triangle defined by the three remaining nearest-neighbor Ga atoms. The final N-Ga bond length is 1.89 Å which is close to the experimental value of 1.95 Å in pure GaN. The relaxed site of the nitrogen atom is within 0.001 Å in a symmetrical position with reference to the gallium atoms, but 0.76 Å out of the Ga plane [see dashed line in Fig. 8(b)]. Consequently, the final geometry of the NV center from DFT strongly supports the C_{3v} symmetry which has been found from the piezospectroscopic experiments.

The vibrational frequencies for the transverse modes of the different isotopic configurations, calculated by DFT using finite displacement of all 63 atoms and measured by FTIR, turned out to be in an almost perfect agreement, thereby further confirming the interpretation of FTIR results as discussed in Sec. III B. The average deviation is less than 2%. Scaling was performed using the formula described in Sec. II. The final frequencies scaled with the factor of 0.9862 are documented in Table I. It should be mentioned that the longitudinal mode frequency, with the eigenvector oriented along the direction of the nitrogen-vacancy axis, is at about 310 cm^{-1}. This mode could not be detected experimentally because it is too close to the strong optical-phonon absorption band.

The relaxation to the minimum of energy for charged super cells leaves the position of the nitrogen atom relative to the lattice atoms unchanged within a limit of 0.001 Å. The result indicates that the additional or removed electrons for charging the super cell are not localized close to NV center.

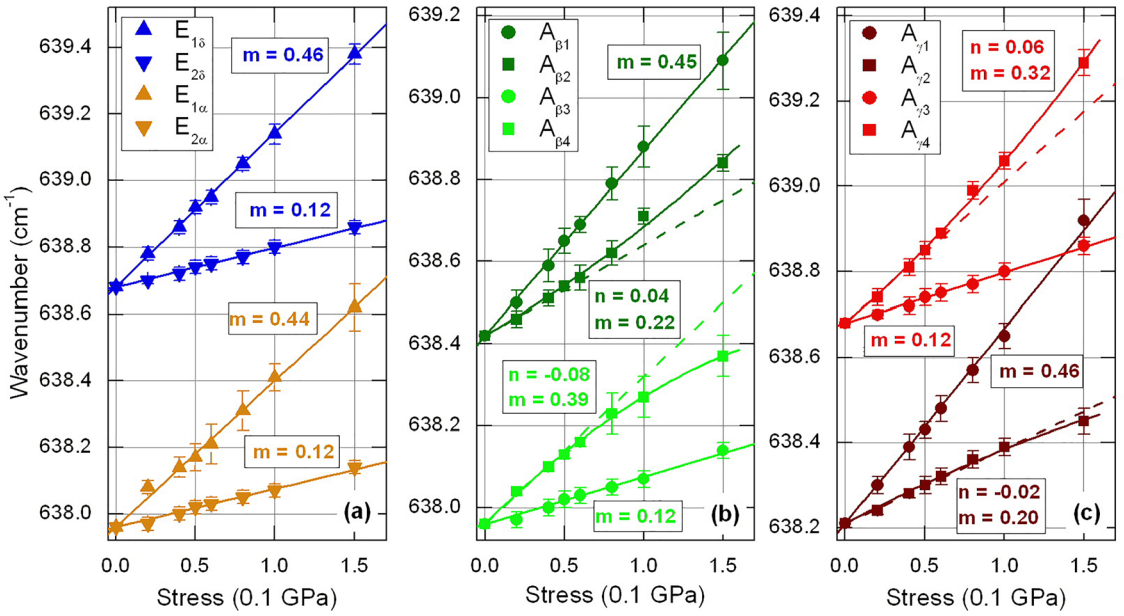

FIG. 7. Shifts and splittings of all components of the 638 cm^{-1}-band: Isotopically pure configurations are shown in (a) and mixed in (b) and (c). The solid curves are fitted second-order polynomials, whereas the initial slopes of the non-linear branches are additionally outlined by dashed straight lines. Coefficients of linear and quadratic terms are referred to as m and n.

This could also be confirmed by analyzing the Hirshfeld charges of the DFT calculations. Furthermore, the two LVM frequencies of the N atom (transverse and longitudinal mode) from DFT calculations vary not more than 0.5% for the different charge states.

Formation energies, calculated by DFT using the LDA exchange-correlation functional, are shown in Fig. 9. Apart from a small range up to about 0.1 eV above the valence band edge, the –3 charge state has the lowest formation energy for all Fermi levels. No deep states are found in the bandgap. From these calculations, the –3 charge state is preferred in thermodynamic equilibrium and is the charge state behind the 638 cm^{-1}-band. However, it should be noted that the DFT calculations are carried out using LDA, which is known to underestimate the bandgap and the localization of the electrons. These underestimations can affect the positions of the charge transition levels. It appears that the –3 charge state is dominated by the Ga vacancy. Both positron annihilation experiments and DFT calculations find that the –3 charge state is prevailing for intrinsic and n-type GaAs.[33,34] The influence of the isoelectronic N atom obviously is of minor importance.

TABLE II. Piezospectroscopic parameters of the components of the 638 cm^{-1}-band as determined from the polynomial fit of the stress-induced shifts.

Mode	Piezospectr. parameters (cm^{-1}/GPa)	
E (α)	$A_\alpha = +2.8$	$B_\alpha = -0.8$
E (δ)	$A_\delta = +2.9$	$B_\delta = -0.9$
A′ (β)	$A_{\beta1} = 4.5$	$A_{\beta2} = 2.2$[a]
A″ (β)	$A_{\beta3} = 1.2$	$A_{\beta4} = 3.9$[a]
A′ (γ)	$A_{\gamma1} = 4.6$	$A_{\gamma2} = 2.0$[a]
A″ (γ)	$A_{\gamma3} = 1.2$	$A_{\gamma4} = 3.2$[a]

[a]Initial slope for $\sigma < 0.05$ GPa.

IV. CONCLUSION

Piezospectroscopic FTIR studies have been carried out on the 638 cm^{-1}-LVM of the $N_{As} - V_{Ga}$ nearest-neighbor pair in GaAs, the nitrogen-vacancy (NV) center. The LVM originates from the vibrational motion of the N atom perpendicular to the $N_{As} - V_{Ga}$ axis. The statistical occupation of the remaining three nearest-neighbor cation lattice sites with the naturally occurring gallium isotopes ^{69}Ga and ^{71}Ga leads to different isotopic configurations. In isotopically pure configurations, this (transverse) LVM is twofold degenerate (E mode) and shows for $\langle 100 \rangle$ stress a splitting behavior typical for $A \rightarrow E$ transitions in centers of C_{3v} symmetry. In the case of the mixed-isotope configurations (non-degenerate A' and A'' modes), the lattice deformation caused by the applied stress interacts with the perturbation due to the isotope anisotropy because both effects are of the same order of magnitude. The resulting dynamical problem has been simulated with the help of a valence-force model. It is found that in some of the mixed-isotope configurations a significant rotation of the vibrational eigenvector and, consequently, stress-induced nonlinear frequency shifts and intensity

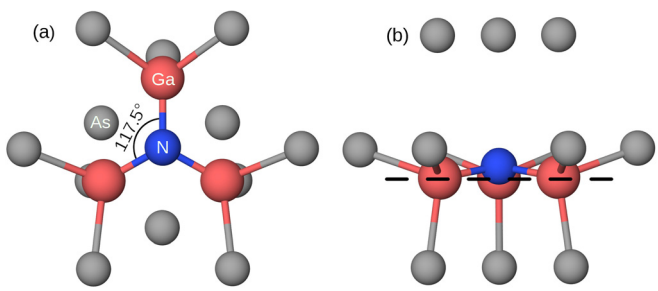

FIG. 8. Local structure of the NV center in the GaAs host crystal after relaxation of the atomic positions with DFT. The N-Ga bond lengths are 1.89 Å (a), the distance between N and the Ga plane (dashed line) is 0.76 Å (b).

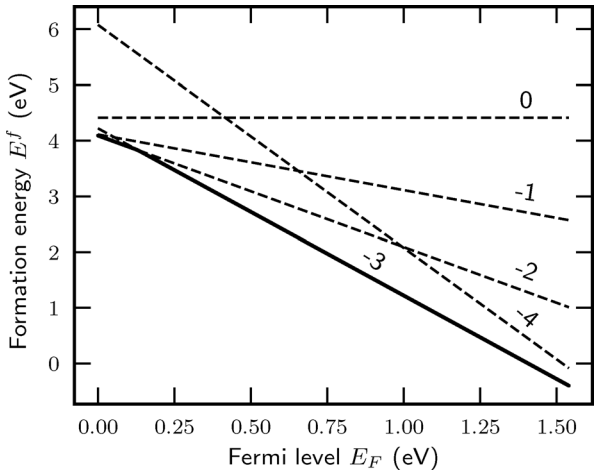

FIG. 9. Formation energy of the NV complex in GaAs calculated with DFT. The numbers indicate the charge state q/e. Positive charge states are not shown since all of them are unstable.

changes have to be taken into account. However, including these effects into the analysis of the piezospectroscopic results, a complete agreement between experimentally observed and fitted absorption spectra can be achieved.

DFT calculations on the NV complex in GaAs turned out to match the experimentally predicted C_{3v} symmetry. The N atom relaxes from the anion lattice site towards a symmetrical position with respect to the three nearest-neighbor Ga atoms. Nitrogen forms strong bonds with these Ga atoms, resulting in a triangular, nearly planar NGa_3 structure. The N-Ga bond length in this minimum-energy structure is close to the value in pure GaN. Furthermore, calculated formation energies show that the –3 charge state is lowest in energy. The NV complex has no deep defect levels in the bandgap. Finally, the calculated vibrational frequency for the transverse mode is very close to the experimental value. The host isotope fine structure is reproduced perfectly. Thereby, frequency calculations further support the identification of the NV complex with the defect responsible for the 638 cm^{-1}-LVM. Overall, the results from FTIR experiments and DFT calculations in this work are in excellent agreement.

ACKNOWLEDGMENTS

The authors are indebted to W. Ulrici for the supply of GaAs samples. The Gauss Centre for Supercomputing e.V. (www.gauss-centre.eu) is gratefully acknowledged for funding this project by providing computing time on the GCS Supercomputer SuperMUC at Leibniz Supercomputing Center (LRZ, www.lrz.de).

[1]M. Weyers, M. Sato, and H. Ando, Jpn. J. Appl. Phys., Part 2 **31**, L853 (1992).
[2]M. Kondow, T. Kitatani, S. Nakatsuka, M. Larson, K. Nakahara, Y. Yazawa, M. Okai, and K. Uomi, IEEE J. Sel. Top. Quantum Electron. **3**, 719 (1997).
[3]D. B. Jackrel, S. R. Bank, H. B. Yuen, M. A. Wistey, J. S. Harris, A. J. Ptak, S. W. Johnston, D. J. Friedman, and S. R. Kurtz, J. Appl. Phys. **101**, 114916 (2007).
[4]D. J. Wolford, J. A. Bradley, K. Fry, and J. Thompson, in *Proceedings of the 17th International Conference on the Physics of Semiconductors* (Springer, New York, NY, 1985), pp. 627–630.
[5]X. Liu, M.-E. Pistol, L. Samuelson, S. Schwetlick, and W. Seifert, Appl. Phys. Lett. **56**, 1451 (1990).
[6]S. Francoeur, J. F. Klem, and A. Mascarenhas, Phys. Rev. Lett. **93**, 067403 (2004).
[7]M. Ikezawa, Y. Sakuma, L. Zhang, Y. Sone, T. Mori, T. Hamano, M. Watanabe, K. Sakoda, and Y. Masumoto, Appl. Phys. Lett. **100**, 042106 (2012).
[8]M. Ikezawa, L. Zhang, Y. Sakuma, and Y. Masumoto, Appl. Phys. Lett. **110**, 152102 (2017).
[9]P. R. C. Kent and A. Zunger, Phys. Rev. B **64**, 115208 (2001).
[10]A. Janotti, S.-H. Wei, S. B. Zhang, S. Kurtz, and C. G. Van de Walle, Phys. Rev. B **67**, 161201 (2003).
[11]S. G. Spruytte, C. W. Coldren, J. S. Harris, W. Wampler, P. Krispin, K. Ploog, and M. C. Larson, J. Appl. Phys. **89**, 4401 (2001).
[12]J. Toivonen, T. Hakkarainen, M. Sopanen, H. Lipsanen, J. Oila, and K. Saarinen, Appl. Phys. Lett. **82**, 40 (2003).
[13]A. H. Kachare, W. G. Spitzer, A. Kahan, F. K. Euler, and T. A. Whatley, J. Appl. Phys. **44**, 4393 (1973).
[14]H. Alt, B. Wiedemann, and K. Bethge, Mater. Sci. Forum **258–263**, 867 (1997).
[15]G. Gärtner, T. Flade, M. Jurisch, A. Köhler, J. Korb, U. Kretzer, and B. Weinert, J. Cryst. Growth **198–199**, 355 (1999).
[16]H. C. Alt, Y. V. Gomeniuk, and B. Wiedemann, Phys. Rev. B **69**, 125214 (2004).
[17]W. Ulrici, F. M. Kiessling, and P. Rudolph, Phys. Status Solidi B **241**, 1281 (2004).
[18]V. Blum, R. Gehrke, F. Hanke, P. Havu, V. Havu, X. Ren, K. Reuter, and M. Scheffler, Comput. Phys. Commun. **180**, 2175 (2009).
[19]F. Knuth, C. Carbogno, V. Atalla, V. Blum, and M. Scheffler, Comput. Phys. Commun. **190**, 33 (2015).
[20]A. Marek, V. Blum, R. Johanni, V. Havu, B. Lang, T. Auckenthaler, A. Heinecke, H.-J. Bungartz, and H. Lederer, J. Phys.: Condens. Matter **26**, 213201 (2014).
[21]T. Auckenthaler, V. Blum, H.-J. Bungartz, T. Huckle, R. Johanni, L. Krämer, B. Lang, H. Lederer, and P. Willems, Parallel Comput. **37**, 783 (2011).
[22]V. Havu, V. Blum, P. Havu, and M. Scheffler, J. Comput. Phys. **228**, 8367 (2009).
[23]J. P. Perdew and Y. Wang, Phys. Rev. B **45**, 13244 (1992).
[24]C. Freysoldt, B. Grabowski, T. Hickel, J. Neugebauer, G. Kresse, A. Janotti, and C. G. Van De Walle, Rev. Mod. Phys. **86**, 253 (2014).
[25]G. Makov and M. C. Payne, Phys. Rev. B **51**, 4014 (1995).
[26]A. Stukowski, Modell. Simul. Mater. Sci. Eng. **18**, 015012 (2010).
[27]A. Togo and I. Tanaka, Scr. Mater. **108**, 1 (2015).
[28]K. K. Irikura, R. D. Johnson, and R. N. Kacker, J. Phys. Chem. A **109**, 8430 (2005).
[29]A. A. Kaplyanskii, Opt. Spectrosc. **16**, 329 (1964).
[30]A. E. Hughes and W. A. Runciman, Proc. Phys. Soc. **90**, 827 (1967).
[31]G. Davies and M. H. Nazare, J. Phys. C: Solid State Phys. **13**, 4127 (1980).
[32]B. B. Nielsen and H. G. Grimmeiss, Phys. Rev. B **40**, 12403 (1989).
[33]J. Gebauer, M. Lausmann, F. Redmann, R. Krause-Rehberg, H. S. Leipner, E. R. Weber, and P. Ebert, Phys. Rev. B **67**, 235207 (2003).
[34]F. El-Mellouhi and N. Mousseau, Phys. Rev. B **71**, 125207 (2005).